J. Fluid Mech. (2004), *vol.* 504, *pp.* 73–97.
DOI: 10.1017/S0022112004008213 Printed in the United Kingdom

Progress-variable approach for large-eddy simulation of non-premixed turbulent combustion

By CHARLES D. PIERCE† AND PARVIZ MOIN

Center for Turbulence Research, Stanford University, Stanford, CA 94305-3030, USA

(Received 30 June 2003 and in revised form 3 December 2003)

A new approach to chemistry modelling for large-eddy simulation of turbulent reacting flows is developed. Instead of solving transport equations for all of the numerous species in a typical chemical mechanism and modelling the unclosed chemical source terms, the present study adopts an indirect mapping approach, whereby all of the detailed chemical processes are mapped to a reduced system of tracking scalars. Here, only two such scalars are considered: a mixture fraction variable, which tracks the mixing of fuel and oxidizer, and a progress variable, which tracks the global extent of reaction of the local mixture. The mapping functions, which describe all of the detailed chemical processes with respect to the tracking variables, are determined by solving quasi-steady diffusion-reaction equations with complex chemical kinetics and multicomponent mass diffusion. The performance of the new model is compared to fast-chemistry and steady-flamelet models for predicting velocity, species concentration, and temperature fields in a methane-fuelled coaxial jet combustor for which experimental data are available. The progress-variable approach is able to capture the unsteady, lifted flame dynamics observed in the experiment, and to obtain good agreement with the experimental data, while the fast-chemistry and steady-flamelet models both predict an attached flame.

1. Introduction

In large-eddy simulation (LES), the large, energy-containing scales of motion are simulated numerically, while the small, unresolved subgrid scales and their interactions with the large scales are modelled. The large scales, which usually control the behaviour and statistical properties of a turbulent flow, tend to be geometry and flow dependent, whereas the small scales tend to be more universal and consequently easier to model.

However, this fundamental advantage of LES has been called into question for reacting flows. It has been argued that since chemical reactions take place only after the reactants become mixed at the molecular level (so that reactions occur mostly in the subgrid scales), turbulent reacting flows cannot, in general, be universal at the smallest scales and therefore, subgrid models for chemical reactions cannot be any simpler than in Reynolds-averaged approaches.

† Charles Pierce died on 25 March 2002.

The counterargument is that the presence of chemical reactions does not invalidate the hypothesis of universality of the small scales. Indeed, flamelet models of turbulent combustion presuppose that there exist universal flame structures at the smallest scales. One could also argue that it is because of the inaccurate modelling of the large scales, in particular large-scale mixing, that Reynolds-averaged approaches sometimes fail to predict turbulent reacting flows accurately, so that even with a fairly simple model for the chemistry, LES may be able to outperform Reynolds-averaged computations that employ more sophisticated chemistry models.

Large-eddy simulation has been developed and studied as a turbulent flow prediction tool for engineering during the past three decades, with significant progress occurring more recently with advances in computer technology and the development of the dynamic subgrid-scale modelling procedure (Germano *et al.* 1991). With the dynamic procedure, model coefficients are automatically computed using information contained in the resolved turbulence scales, thereby eliminating the uncertainties associated with tunable model parameters. Moin *et al.* (1991) applied the dynamic procedure to scalar transport and subgrid kinetic energy models for compressible turbulent flows using Favre filtering. Reviews of LES are given by Lesieur & Métais (1996) and Moin (2002). The application of large-eddy simulation to chemically reacting flows has been a subject of growing interest, but to date few simulations of realistic combustion systems have been undertaken.

The application of LES to gas turbine combustor configurations has been facilitated by the availability of comprehensive experimental data for both non-swirling and swirling confined coaxial jets with and without chemical reactions, due to the classic experiments that were conducted at United Technologies Research Center (Johnson & Bennett 1981, 1984; Roback & Johnson 1983; Owen, Spadaccini & Bowman 1976; Spadaccini, Owen & Bowman 1976). Akselvoll & Moin (1996) simulated incompressible flow with a passive scalar in a non-swirling confined coaxial jet and obtained good agreement with the experiment of Johnson & Bennett (1984). Pierce & Moin (1998*a*) further extended that work to include the effects of swirl, which is commonly used in gas-turbine combustors, and chemical heat release, which requires the use of variable-density transport equations. These studies were successful in predicting velocity and conserved-scalar mixing fields in complex combustor flows, but they did not consider the effects of finite-rate chemistry or the general issue of chemistry modelling in LES.

Techniques for computational modelling of turbulent combustion have been the subject of numerous studies, with significant advances attributable to the development of flamelet models (Peters 1984, 1986), probability density function (PDF) methods (Pope 1985, 1990), conditional moment closure (Klimenko & Bilger 1999), and linear eddy modelling (Kerstein 1992*a*, 1992*b*; McMurtry *et al.* 1993; Calhoon and Menon 1996). A comprehensive review of turbulent combustion modelling has been written by Peters (2000). Many of these established modelling approaches have recently been extended for use in large-eddy simulations.

The steady-flamelet model was proposed for LES and tested in homogeneous turbulence by Cook, Riley & Kosály (1997). Unsteady-flamelet modelling was used by Pitsch & Steiner (2000) in large-eddy simulation of a piloted jet diffusion flame, where excellent agreement with the experimental data was obtained. Gao & O'Brien (1993), Réveillon & Vervisch (1998), among others, have proposed extensions of the PDF method to LES. In the latter study, the dynamic approach was used to close the turbulent micro-mixing term in the PDF transport equation. Monte Carlo simulation techniques, which are commonly used in the implementation of PDF methods, have

been generalized to LES via the filtered density function (Colucci *et al.* 1998; Jaberi *et al.* 1999). A variant of the conditional moment closure technique, called conditional source estimation was proposed by Bushe & Steiner (1999), who also incorporated it into an LES of a piloted jet diffusion flame (Steiner & Bushe 2001). Jaberi & James (1998) proposed modelling the filtered chemical source terms in LES using the scale-similarity approach and obtained the corresponding model coefficient using the dynamic procedure. However, scale-similarity assumptions may be inappropriate for quantities that are dominated by small scales such as chemical reactions and scalar dissipation, and therefore, it is unlikely that extrapolation from larger scales would yield accurate results in high Reynolds number applications. DesJardin & Frankel (1998) have performed an extensive evaluation of several subgrid-scale combustion models. However, since these simulations were two-dimensional, their conclusions may not be applicable to LES of high Reynolds number flows.

Assumed PDF methods offer a simple and inexpensive alternative to modelling approaches that solve PDF transport equations (Frankel *et al.* 1993). The most important application of assumed PDFs has been in the modelling of mixture fraction fluctuations. Cook & Riley (1994) proposed the assumed beta PDF as a subgrid-scale mixing model in LES and successfully tested it in homogeneous turbulence. Jiménez *et al.* (1997) tested the assumed beta PDF for LES in a turbulent mixing layer and demonstrated, in particular, the superior performance of the model in highly intermittent, forced mixing layers where the assumed PDF approach in the Reynolds-averaged Navier–Stokes (RANS) context was found to be very inaccurate. Wall, Boersma & Moin (2000) tested the model in the presence of chemical heat release and also demonstrated that good results can be obtained. Assumed PDFs require the variance of the subgrid scalar fluctuations as an input parameter. This quantity was modelled by Cook & Riley (1994) using a scale-similarity assumption. A theoretical estimate for the coefficient in this model was obtained by Cook (1997) and Jiménez *et al.* (1997). Pierce & Moin (1998*c*), using equilibrium assumptions for the subgrid scales, obtained an algebraic scaling law for the variance and computed its coefficient using the dynamic procedure.

One of the major challenges faced during the present study was to predict flame lift-off in non-premixed combustion. The flamelet/progress-variable approach, introduced by Pierce & Moin (2001) and described in the following sections, was developed in part to address this problem. The concept of a reaction progress variable is not new to combustion modelling, indeed progress variables are frequently employed to describe chemistry in premixed and partially premixed flames. Recently, progress variables have been combined with flamelet methods to model premixed counterflow flames (van Oijen & de Goey 2002) and flames burning in a two-dimensional turbulent wake (Domingo, Vervisch & Bray 2002). To the authors' knowledge, the current work is the first attempt to use such an approach in a fully three-dimensional LES of a non-premixed combustion system.

Additionally, it should be mentioned that an alternative method to predict lift-off may be to use the level-set or G-equation approach in combination with mixture fraction. This was used by Müller, Breitbach & Peters (1994) and Chen, Herrmann & Peters (2000) in RANS calculations of lifted jet flames. Other approaches for modelling partially premixed combustion and lifted flames in LES have also been proposed (Vervisch & Trouvé 1998; Legier, Poinsot & Veynante 2000).

The objective of this work is the development of a large-eddy-simulation-based prediction methodology for turbulent reacting flows with principal application to gas turbine combustors.

2. Turbulence model

In this work, solutions to the reacting flow equations are obtained using the technique of large-eddy simulation. The large, energy-containing scales of motion are simulated numerically while the small, unresolved scales and their interactions with the large scales are modelled.

2.1. *Filtered LES equations*

In LES, all of the field variables can be decomposed into resolved and subgrid-scale parts. The resolved, large-scale fields are related to the instantaneous full-scale fields through a grid-filtering operation that removes scales too small to be resolved by the simulation.

The LES equations for the resolved fields can be formally derived by substituting this decomposition into the governing equations, and then subjecting the equations to the grid filter. The instantaneous small-scale fluctuations are removed by the filter, but their statistical effects remain in unclosed residual terms representing the influence of the subgrid scales on the resolved scales. Applying this procedure to the low-Mach-number form of the governing flow equations, the LES equations are written as

continuity:

$$\overline{\rho}_{,t} + (\overline{\rho}\widetilde{u}_j)_{,j} = 0, \tag{1}$$

momentum:

$$\begin{gathered}(\overline{\rho}\widetilde{u}_i)_{,t} + (\overline{\rho}\widetilde{u}_i\widetilde{u}_j)_{,j} = -\overline{p}_{,i} + (2\overline{\mu}\widetilde{S}_{ij})_{,j} + t_{ij,j}, \\ \widetilde{S}_{ij} = \tfrac{1}{2}(\widetilde{u}_{i,j} + \widetilde{u}_{j,i}) - \tfrac{1}{3}\delta_{ij}\widetilde{u}_{k,k},\end{gathered} \tag{2}$$

scalar transport:

$$(\overline{\rho}\widetilde{\phi}_i)_{,t} + (\overline{\rho}\widetilde{u}_j\widetilde{\phi}_i)_{,j} = (\overline{\rho}\widetilde{\alpha}_i\widetilde{\phi}_{i,k})_{,k} + \overline{\rho}\widetilde{w}_i + q_{ik,k}, \tag{3}$$

state relation:

$$\overline{\rho} = \overline{f(\phi_1, \phi_2, \ldots)}. \tag{4}$$

Here, ρ is the density, u_j is the velocity vector, p is the pressure, μ is the dynamic viscosity, δ_{ij} is the Kronecker symbol, ϕ_i represents scalar quantities, α_i is the diffusivity of the scalar i, and w_i is the chemical source term of scalar i. The filtering operation is denoted by an overbar and Favre (density-weighted) filtering by a tilde. Subscript notation has been used for partial derivatives. All unclosed transport terms in the momentum and scalar equations are grouped into the residual stress, t_{ij}, and residual scalar flux, q_{ik}. These terms as well as the filtered chemical source terms, $\widetilde{w}_i$, and the state relation require closure modelling.

2.2. *Subgrid-scale models*

2.2.1. *Turbulent stress and scalar flux*

Subgrid momentum and scalar transport terms that appear in (2) and (3) are modelled using the dynamic approach of Moin *et al.* (1991). The present formulation differs from Moin *et al.* in the use of the deviatoric strain rate for the definition of $|\widetilde{S}|$ and in the use of least-squares averaging.

The residual stresses are modelled as subgrid turbulent stresses with an eddy viscosity assumption,

$$t_{ij} = -\overline{\rho}\widetilde{u_i u_j} + \overline{\rho}\widetilde{u}_i\widetilde{u}_j = 2\mu_t\widetilde{S}_{ij} - \tfrac{1}{3}\overline{\rho}q^2\delta_{ij}, \tag{5}$$

where $\frac{1}{2}\overline{\rho}q^2$ is the subgrid kinetic energy and $\widetilde{S}_{ij}$ is defined under (2).

The eddy viscosity is given by the Smagorinsky model,

$$\mu_t = C_\mu \overline{\rho} \Delta^2 |\widetilde{S}|, \quad \text{where} \quad |\widetilde{S}| = \sqrt{\widetilde{S}_{ij}\widetilde{S}_{ij}}, \tag{6}$$

and the subgrid kinetic energy is modelled using

$$\overline{\rho} q^2 = C_k \overline{\rho} \Delta^2 |\widetilde{S}|^2, \tag{7}$$

where Δ is the filter width. Note, that the isotropic part of the residual stress does not need to be modelled separately when pressure is decoupled from thermodynamic variables, because it may then be lumped together with the pressure. In the present study, acoustic interactions and compressibility are neglected, so in the interest of computational efficiency, this term is not actually computed.

The residual scalar fluxes are modelled as subgrid turbulent scalar fluxes with a gradient-diffusion assumption,

$$q_{ik} = -\overline{\rho}\widetilde{u_k \phi_i} + \overline{\rho}\,\widetilde{u}_k \widetilde{\phi}_i = \overline{\rho}\alpha_t \widetilde{\phi}_{i,k}, \tag{8}$$

where the eddy diffusivity is given by

$$\overline{\rho}\alpha_t = C_\alpha \overline{\rho} \Delta^2 |\widetilde{S}|. \tag{9}$$

Note that the eddy diffusivity model has the same algebraic form as the eddy viscosity model, but the model coefficient is different. The ratio of the two coefficients gives the subgrid turbulent Prandtl number, $Pr_t = C_\mu / C_\alpha$. The coefficients in all of these models, C_μ, C_k, and C_α, are evaluated using the dynamic procedure.

2.2.2. *Variance for a conserved scalar*

Subgrid scalar variance is an input parameter to the assumed PDF model discussed in the following section. Following Pierce & Moin (1998*c*), starting from assumptions of local homogeneity and local equilibrium for the subgrid scales, an algebraic model for the subgrid variance can be derived. The subgrid variance is modelled using

$$\overline{\rho}\widetilde{\phi''^2} = C_\phi \overline{\rho} \Delta^2 |\nabla \widetilde{\phi}|^2 \tag{10}$$

The coefficient C_ϕ is determined dynamically.

2.2.3. *Assumed beta PDF for a conserved scalar*

While algebraic scaling laws and scale-similarity concepts can be expected to work for quadratic nonlinearities, the only acceptable closure for arbitrary nonlinearities appears to be the subgrid probability density function (PDF) approach. When Favre filtering is used for the scalar variables, filtered quantities $\widetilde{y}$ should be evaluated using the joint Favre subgrid PDF $\widetilde{P}(\phi_1, \phi_2, \ldots)$ of the subgrid scalar fluctuations as

$$\widetilde{y} = \int y(\phi_1, \phi_2, \ldots) \widetilde{P}(\phi_1, \phi_2, \ldots)\, \mathrm{d}\phi_1\, \mathrm{d}\phi_2 \ldots, \tag{11}$$

where the density-weighted Favre PDF is related to the standard PDF by

$$\widetilde{P}(\phi_1, \phi_2, \ldots) = \frac{\rho(\phi_1, \phi_2, \ldots) P(\phi_1, \phi_2, \ldots)}{\overline{\rho}}. \tag{12}$$

The Reynolds-filtered density can be obtained using $\widetilde{P}$ by dividing (12) by ρ and integrating, with the result that,

$$\overline{\rho} = \left[\int \frac{\widetilde{P}(\phi_1, \phi_2, \ldots)}{\rho(\phi_1, \phi_2, \ldots)}\, \mathrm{d}\phi_1\, \mathrm{d}\phi_2 \ldots \right]^{-1}. \tag{13}$$

In the assumed subgrid PDF method, the subgrid PDF (also known as the filtered density function) is modelled directly using simple analytical forms, such as the beta distribution. However, because source terms can directly modify the subgrid PDF of a scalar, the beta distribution can be expected to be valid only for conserved scalars. For this reason, in this work it is applied only to mixture fraction Z.

The two-parameter family of beta distributions on the interval $0 \leqslant x \leqslant 1$ is given by

$$P(x;a,b) = x^{a-1}(1-x)^{b-1}\frac{\Gamma(a+b)}{\Gamma(a)\Gamma(b)}, \tag{14}$$

where the parameters a and b are related to the distribution of mean and variance (μ, σ^2) by

$$a = \frac{\mu(\mu - \mu^2 - \sigma^2)}{\sigma^2}, \qquad b = \frac{(1-\mu)(\mu - \mu^2 - \sigma^2)}{\sigma^2}.$$

When applied to mixture fraction, $x \to Z$, $\mu \to \widetilde{Z}$, and $\sigma^2 \to \widetilde{Z''^2}$.

Closures for the filtered chemical source terms and the state relation, which are related to the chemical model, are discussed in the following section.

3. Chemistry models

Developing effective strategies for incorporating chemistry into large-eddy simulations is the main objective of this paper. The straightforward, brute-force approach would be to find a suitable chemical kinetic mechanism for the system under investigation, solve scalar transport equations for all the species in the mechanism, and attempt to model the filtered source term in each equation.

A serious problem with this direct approach is that realistic kinetic mechanisms can involve tens of species and hundreds of reaction steps, even for 'simple' fuels such as methane. Unless mechanism reduction methodologies can drastically reduce the dimensionality of the chemical system, one is faced with having to solve a large number of stiffly coupled scalar transport equations.

Another problem is that each species transport equation contains a filtered chemical source term that must be modelled. Like the state relation (4), each chemical source term is, in principle, an arbitrary nonlinear function of the scalar variables. As discussed in the previous section, subgrid PDF methods are the most attractive approach for evaluating such nonlinearities; however, when the number of independent variables becomes large (say, more than three) joint subgrid PDFs can become unwieldy.

Thus, the key to combustion modelling in LES appears to be minimizing the number of transported scalar variables required. For non-premixed combustion, mixture-fraction-based models appear to offer the most effective description of the chemistry. By mapping the details of the multicomponent diffusion-reaction processes to a small number of 'tracking' scalars, complete chemical state information can be obtained at greatly reduced computational expense.

The philosophy underlying the chemical models developed in this work is that the most effective description of turbulent combustion will map the details of the multicomponent diffusion-reaction processes to a minimum set of transported 'tracking' scalars. For combustion processes, which are essentially non-premixed, an obvious choice for such a scalar is the mixture fraction. However, a model based on mixture fraction alone is incomplete, because mixture fraction does not contain any intrinsic information about chemical reactions. At least one additional scalar is needed, and

since mixture fraction accounts for transport of conserved scalars, additional tracking scalars must be non-conserved in order to be independent from mixture fraction. A non-conserved tracking scalar is best characterized as a reaction progress variable. In the following, we will first outline key aspects of the chemistry model used in this study, then provide a transport equation for the reaction progress variable, and finally propose a simple closure model for the chemical source term appearing in that equation, using a presumed subgrid PDF approach.

In the present study, combustion chemistry is incorporated in the form of a steady-state one-dimensional flamelet model. The flamelet equations are formulated and solved in physical space rather than in mixture-fraction space as is done in traditional flamelet methods. Once the physical-space equations have been solved, the mixture fraction is determined from the resulting element mass fractions, and the solution is mapped to the mixture fraction. The physical-space (x-coordinate) steady-flamelet equations (including Soret and Dufour effects) are

$$\left.\begin{aligned} \rho u y_{i,x} &= -(\rho y_i V_i)_{,x} + \rho w_i, \\ \rho u h_{,x} &= \left(\kappa T_{,x} - \sum_i \rho V_i y_i h_i - q_D\right)_{,x}, \\ h &= \sum_i y_i h_i(T), \\ \rho &= p_0 \Big/ \sum_i \frac{y_i}{M_i} \hat{R} T, \end{aligned}\right\} \tag{15}$$

where V_i is the diffusion velocity of species i, h_i is the enthalpy of species i, h is the total enthalpy, κ is the thermal conductivity, and q_D is the heat flux associated with Dufour diffusion.

In order to solve (15), the velocity $u(x)$ must be prescribed. The standard flamelet approach (Peters 1984; Cook *et al.* 1997) usually assumes a counterflow configuration with $u(x) = -Sx$, where S is the strain rate. While the counterflow configuration does lead to an essentially one-dimensional diffusion flame structure, it cannot serve as a valid model along the entire flame surface. Indeed, to assume that a flame burning in an unsteady mixing layer is subjected to local counterflow at every point on its surface violates the continuity equation. On physical grounds, a proportionate amount of flame surface must experience local reverse-counterflow in order to conserve mass. The counterflow configuration has also been proposed to account for self-similar thickening of the flame over time with $Z_{,t} = -(Sx)Z_{,x}$, where in this case S is the thickening rate. However, there is little reason to expect this to be valid in a turbulent flow, where mixing layers are constantly subjected to varying strain rates at different Z locations. The counterflow assumption places an undue bias on the flamelet solutions by imposing very specific velocity profiles, $u(x)$, and corresponding profiles, $\chi(Z)$, of the scalar dissipation rate, χ, which is defined by $\chi = 2D|\nabla Z|^2$, where D is the scalar diffusivity. In a turbulent flow, where both the velocity field and dissipation rate fluctuate strongly, the dissipation rate is usually not correlated with mixture fraction. In the absence of a stochastic description of $u(x)$ or $\chi(Z)$, the most unbiased assumption is $u(x) = 0$ or $\chi(Z) \simeq$ constant.

With the assumption $u(x) = 0$, the flamelet equations can be regarded as pure diffusion-reaction equations. The length scale of the flame is set by imposing Dirichlet boundary conditions on species and enthalpy at the ends of a finite domain of length L. The point $x = 0$ corresponds to oxidizer stream conditions, while fuel stream conditions are enforced at $x = L$. By varying the domain length, L, a one-parameter

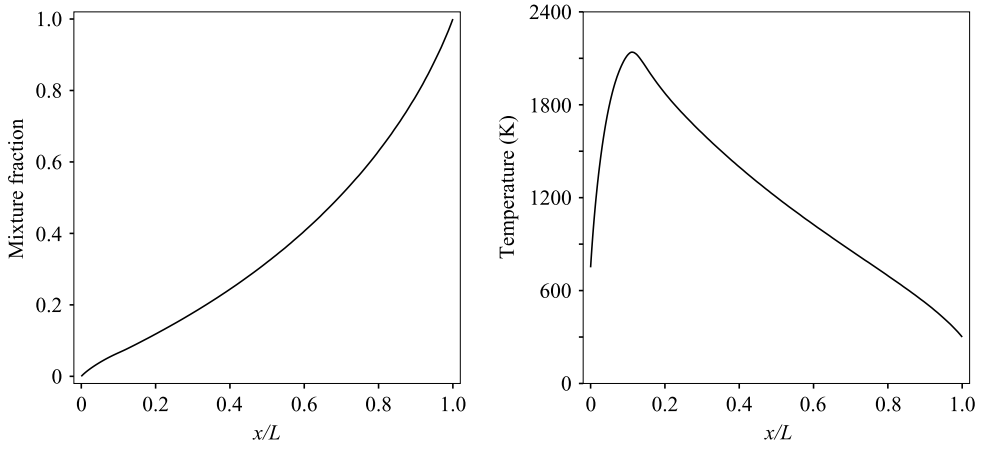

FIGURE 1. Mixture fraction and temperature from a steady-flamelet solution in physical space. Methane–air combustion at the conditions of the experiment in § 5 (750 K air, 300 K fuel, 3.8 atm). $L = 0.2$ cm.

family of steady-flamelet solutions is obtained. The entire family of solutions is compiled into a flamelet library.

This configuration does give rise to an inconsistency at the endpoints, $x = 0$ and $x = L$, where physically, the fluxes must go to zero as they are absorbed by unsteady growth of the mixing layer. In practice, however, this is not expected to cause any problems because in the endpoint fringe regions, the chemical state must approach the fixed inflow stream conditions regardless. A typical flamelet solution in physical space is shown in figure 1. Provided that the mixture fraction solution, $Z(x)$, is a monotonic function of the spatial coordinate, the inverse function $x(Z)$ can be obtained and used to map all of the combustion variables to mixture fraction. The solution dependence on L is mapped to a single progress variable, generically denoted by C. The complete range of flame states, from completely extinguished (mixing without reaction) to completely reacted (equilibrium chemistry), is represented in the library. Arbitrarily complex chemical kinetic mechanisms as well as differential-diffusion effects can be included. The result is a complete set of flame states, given in terms of mixture fraction and the reaction progress variable.

The set of scalar transport equations carried in a simulation is then given by

$$\left.\begin{aligned} \frac{\partial \overline{\rho}\widetilde{Z}}{\partial t} + \nabla\cdot(\overline{\rho}\widetilde{\boldsymbol{u}}\widetilde{Z}) &= \nabla\cdot[\overline{\rho}(\widetilde{\alpha}_Z + \alpha_t)\nabla\widetilde{Z}], \\ \frac{\partial \overline{\rho}\widetilde{C}}{\partial t} + \nabla\cdot(\overline{\rho}\widetilde{\boldsymbol{u}}\widetilde{C}) &= \nabla\cdot[\overline{\rho}(\widetilde{\alpha}_C + \alpha_t)\nabla\widetilde{C}] + \overline{\rho}\widetilde{w}_C, \end{aligned}\right\} \tag{16}$$

where α_t is the turbulent diffusivity. To account for subgrid fluctuations in the mixture fraction and progress variable, filtered combustion variables are obtained by integrating chemical state relationships over the joint subgrid PDF of Z and C. As an example, for the filtered species mass fractions $\widetilde{y}_i$ and the filtered chemical source term of the progress variable this leads to

$$\widetilde{y}_i = \int y_i(Z, C)\widetilde{P}(Z, C)\,\mathrm{d}Z\,\mathrm{d}C, \tag{17}$$

and

$$\widetilde{w}_C = \int w_C(Z, C)\widetilde{P}(Z, C)\,\mathrm{d}Z\,\mathrm{d}C. \tag{18}$$

The chemical state relationships for the mass fractions, the temperature T, the density, and the chemical source term of the progress variable:

$$y_i = y_i(Z, C), \qquad T = T(Z, C), \qquad \rho = \rho(Z, C), \qquad w_C = w_C(Z, C), \tag{19}$$

are obtained from the steady-state flamelet library.

The joint subgrid PDF is modelled by first writing

$$\widetilde{P}(Z, C) = \widetilde{P}(C|Z)\widetilde{P}(Z), \tag{20}$$

where $\widetilde{P}(Z)$ is given by the assumed beta subgrid PDF of § 2.2.3. The conditional subgrid PDF, $\widetilde{P}(C|Z)$, is modelled by assuming that the scale over which a single flamelet solution is valid is greater than or equal to the size of the computational cell; therefore, each subgrid chemical state is represented by a single flamelet solution. Mathematically this is described by a delta function,

$$\widetilde{P}(C|Z) = \delta(C - \widetilde{C|Z}). \tag{21}$$

In (21), the conditional mean, $\widetilde{C|Z}$, is given by the steady-flamelet solution

$$\widetilde{C|Z} = C(Z, \psi_0). \tag{22}$$

Here, ψ is any variable that can be used to parameterize the family of flamelet solutions.

Typically, flamelet solutions are parameterized by the scalar dissipation rate, χ, meaning that the chemical state in the LES is completely described by mixture fraction and scalar dissipation rate. There is no reason, however, why different parameterizations of the family of flamelet solutions could not be used. Instead of the scalar dissipation rate, flamelet solutions could be parameterized by the temperature at the point where the mixture fraction is equal to its stoichiometric value, T_{st}, or by the maximum product mass fraction, y_{Pmax}, as well as a number of other suitable choices. The reference value of the chosen parameter, ψ_0, is chosen such that the constraint

$$\widetilde{C} = \int C(Z, \psi_0)\widetilde{P}(Z)\,\mathrm{d}Z \tag{23}$$

is satisfied. This ensures that the flamelet solution that is chosen for each subgrid cell will be consistent with the value of the progress variable, $\widetilde{C}$, that has been computed from the transport equation for that cell. It is important to note that as long as ψ_0 is chosen such that this constraint is satisfied, the particular choice of parameter, ψ, will not affect the chemistry model, since the functional relationship between C and Z given by $C(Z, \psi_0)$ in (23) will not depend on the choice of the parameter, ψ. The flamelet/progress-variable approach could benefit from a more sophisticated model for $\widetilde{P}(C|Z)$, but as noted in § 2.2.3, assumed subgrid PDF modelling of reacting scalars needs to be further researched.

The implementation of the flamelet/progress-variable approach is similar to the steady-flamelet model in that it employs chemical state relationships determined by a flamelet library and uses assumed subgrid PDFs to represent subgrid fluctuations. The major difference, of course, is the parameterization by a progress variable instead of dissipation rate. Once the flamelet library is computed and assumed subgrid PDF

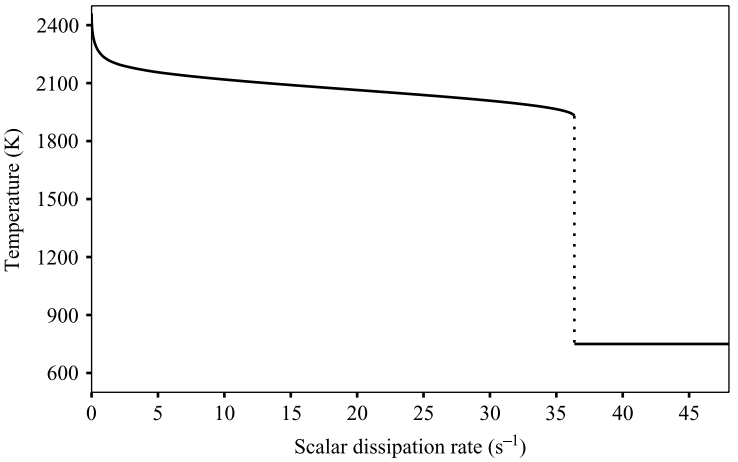

FIGURE 2. Locus of maximum flame temperatures in the steady-flamelet library. Note the discontinuous jump between burning and extinguished solutions at the critical point. Methane–air combustion at the conditions of the experiment in § 5 (750 K air, 300 K fuel, 3.8 atm).

integrals are evaluated, lookup tables can be generated to provide the filtered chemical variables as functions of the quantities readily available from LES (namely, $\widetilde{Z}$, $\widetilde{Z''^2}$, and $\widetilde{C}$):

$$\widetilde{y}_i = \widetilde{y}_i(\widetilde{Z}, \widetilde{Z''^2}, \widetilde{C}), \quad \widetilde{T} = \widetilde{T}(\widetilde{Z}, \widetilde{Z''^2}, \widetilde{C}), \quad \overline{\rho} = \overline{\rho}(\widetilde{Z}, \widetilde{Z''^2}, \widetilde{C}), \quad \text{etc.} \tag{24}$$

Note that (24) includes similar expressions for $\overline{\mu}$, $\widetilde{\alpha}_Z$, $\widetilde{\alpha}_C$, and $\widetilde{w}_C$, which are used in solving the large-scale momentum and scalar transport equations. The computational cost of the flamelet/progress-variable approach is only marginally greater than the steady-flamelet model, because the functions in (24) can be precomputed and tabulated prior to running a simulation. The major additional cost comes from solving the transport equation for the progress variable.

One of the more conspicuous limitations of the steady-flamelet model is its inability to properly account for ignition and extinction phenomena. This is exemplified most clearly by the discontinuous jump in flame states in figure 2, which indicates that the steady-flamelet library is somehow incomplete because it cannot represent any of the 'partially extinguished' intermediate states that should fill the gap between the critical point and complete extinction. In fact, the steady-flamelet equations do provide a complete and continuous set of solutions ranging from chemical equilibrium to complete extinction, but they are not in general uniquely parameterized by the dissipation rate.

The complete locus of solutions to the steady-flamelet equations is shown in figure 3. The shape of this curve, sometimes called the 'S-shaped curve' in diffusion flame theory, is determined primarily by the chemical kinetics. With Arrhenius kinetics, there are typically three solution branches: (i) the steady burning branch, (ii) the unstable branch of partially extinguished states, and (iii) the complete extinction line. On the stable burning branch, maximum flame temperature decreases with increasing dissipation rate as more rapid mixing increases reactant concentrations while diluting product concentrations. When the critical point is reached, the flame temperature becomes so low that Arrhenius rate factors in the chemical kinetics begin to limit reaction rates, even as reactant concentrations continue to increase. Below the

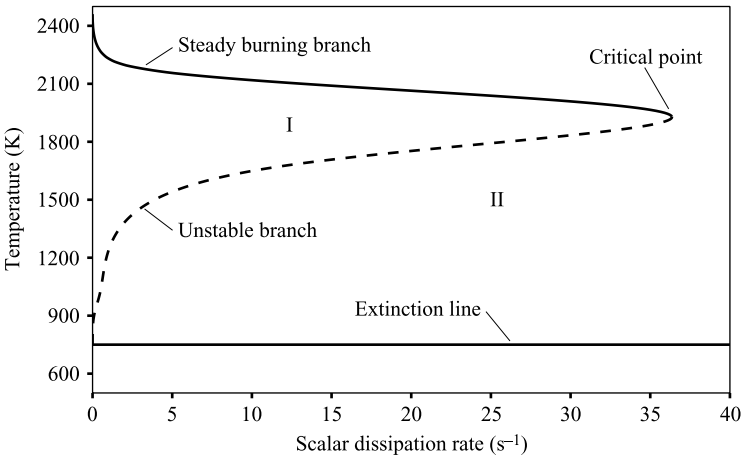

FIGURE 3. Locus of maximum flame temperatures from a complete set of steady-flamelet solutions including the unstable branch. This should be compared with figure 2.

critical point on the unstable branch, dissipation rate must decrease with decreasing flame temperature in order to keep mixing in balance with lower reaction rates at colder temperatures. On the complete extinction line, the effect of chemical kinetics is negligible so that the chemical state is independent of dissipation rate. The flame state that satisfies (23) may be found anywhere on the complete locus of solutions for the flame state found in figure 3; therefore, flame states which are not capable of being represented in the steady-flamelet model may be represented by the progress-variable approach.

In reality neither the locus of solutions shown in figure 2 nor the locus of solutions shown in figure 3 will be able to correctly represent all ignition and extinction phenomena, because these phenomena are inherently unsteady; therefore, they cannot be perfectly represented by models which assume them to be steady. In general, during extinction or ignition, flame states will not follow the discontinuous jump of the steady-flamelet model as shown in figure 2 or the complete set of solutions used in the progress-variable model as shown in figure 3. The progress-variable approach, however, does have two advantages over the steady-flamelet model. First, the progress-variable approach is capable of representing flame states which are completely extinguished, but which are to the left of the critical point in figure 3. The steady-flamelet model cannot represent these states, because for a given value of the scalar dissipation rate, the steady-flamelet model can only represent one flame state. For values of the scalar dissipation which are less than the critical value, the steady-flamelet model only represents the steady burning state. Second, although the path that is followed during extinction or reignition in the progress-variable model is not entirely accurate, it is continuous unlike the path followed in the steady-flamelet model. For these two reasons, the progress-variable approach may be expected to provide a more accurate representation of extinction and reignition phenomena than the steady-flamelet model, although neither describes these phenomena with complete accuracy.

4. Numerical method and boundary conditions

The essential elements of the numerical method can be found in Wall, Pierce & Moin (2002), and details of its implementation in cylindrical coordinates are in Pierce &

Moin (2001). The method is second order in space and time. For this study, we developed and used a staggered space–time, conservative discretization for the low-Mach-number, variable-density transport equations, as well as an efficient, semi-implicit iterative technique for integrating those equations. In the remainder of this section, we describe the numerical boundary conditions used.

The wall boundary conditions used in the present study are Neumann conditions for all scalars and pressure, and no-slip Dirichlet conditions for velocity.

Turbulent inflow conditions for LES must reflect the three-dimensional, unsteady nature of turbulence. In principle, the computational domain should be extended to include all the upstream geometry and flow conditioning devices (such as swirl vanes) that may influence flow properties farther downstream. But because this is usually not practical, approximate inflow conditions must be considered. In many cases, the inflow condition is a developing turbulent duct flow that can be approximated as fully developed. The unsteady inflow conditions can then be generated by simulating a spatially periodic section of the duct. Generalization of this approach to generate swirling inflow conditions is discussed by Pierce & Moin (1998*b*).

In the present study, a separate inflow generation code was used to create an 'inflow database'. The inflow generator simulates a spatially periodic, fully developed, co-axial pipe flow. Every few time steps, a cross-section of velocity data is saved to the inflow database, until sufficient inflow data have been accumulated to provide converged turbulence statistics. In the main simulation, planes of velocity data are read from the inflow database in succession and applied to the inflow boundary. Linear interpolation in both space and time is performed when the inflow database grid and time step do not exactly match the grid and time step of the main simulation. If the end of the database is reached before the simulation is completed, inflow sampling returns to the beginning of the database, thereby recycling turbulent inflow conditions when necessary. This is not expected to cause any problems when the database contains sufficient samples to produce converged statistics and when the main simulation contains flow time scales longer than the inflow recyling interval.

The convective condition is used for all 'outflow' boundaries, which may also include 'open' boundaries where the flow may actually enter the domain, as occurs for example, when ambient fluid is entrained into a free jet. Mathematically, this condition is written

$$\frac{\partial \phi}{\partial t} + c\frac{\partial \phi}{\partial n} = 0, \tag{25}$$

where ϕ is any scalar variable or velocity component, c is the convection velocity, and n is the coordinate in the direction of the outward normal at the boundary. In non-Cartesian coordinates, the normal component of velocity satisfies a slightly modifed form of the convective condition to account for changes in flow area in the direction normal to the boundary. Instead of $\partial u_n/\partial n$, the corresponding term from the continuity equation is used. For example, in cylindrical coordinates, the convective condition for the radial component of velocity at a radially oriented outflow boundary satisfies

$$\frac{\partial u_r}{\partial t} + c\frac{1}{r}\frac{\partial r u_r}{\partial r} = 0. \tag{26}$$

This ensures that the time-average of the ouflow mass flux is the same as the mass flux at the first interior point away from the boundary. Normal derivatives at the outflow boundary are evaluated using one-sided, first-order differences, and the convection velocity is taken to be constant over the outflow boundary.

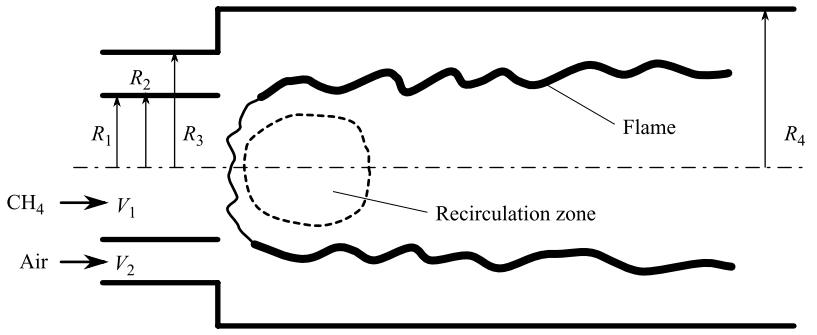

FIGURE 4. Schematic of the coaxial jet combustor experiment.

5. Application to a coaxial jet combustor

Employing the models described in previous sections, numerical simulations have been performed for a methane fuelled coaxial jet combustor. The results are compared with experimental data by Owen *et al.* (1976). In addition, the results are compared with simulations using a fast-chemistry and a steady-state flamelet model under otherwise identical conditions.

The experimental study used for the validation of the simulation methodology was the coaxial jet combustor configuration of Owen *et al.* (1976). This experiment was chosen for its relatively simple geometry and boundary conditions yet complex flow patterns resembling those in a gas turbine combustor, and for the availability of detailed measurements that map the species, temperature, and velocity fields within the combustor. The experimental study consisted of eight test cases conducted under various operating conditions and geometric modifications. The particular case used for the present validation, referred to as 'Test 1' in the laboratory report (Spadaccini *et al.* 1976), is depicted in figure 4.

The configuration had a relatively large-diameter, low-velocity central fuel port, with higher velocity, non-swirling air in a surrounding annulus. The air was preheated to 750 K, and the combustor was pressurized to 3.8 atm. Porous-metal disks were installed in the fuel injector and air entry section to provide uniform inlet flows. The walls of the combustor were water-cooled to maintain a constant wall temperature of roughly 500 K. The dimensions and flow conditions specified in the experiment are summarized below:

central pipe radius (R_1):	3.157 cm
annular inner radius (R_2):	3.175 cm
annular wall thickness ($R_2 - R_1$):	0.018 cm
annular outer radius (R_3):	4.685 cm $\equiv R$
combustor radius (R_4):	6.115 cm
combustor length:	100.0 cm
mass flow rate of fuel:	0.00720 kg s^{-1}
mass flow rate of air:	0.137 kg s^{-1}
bulk velocity of fuel (V_1):	0.9287 m s^{-1}
bulk velocity of air (V_2):	20.63 m s^{-1} $\equiv U$
overall equivalence ratio:	0.9
temperature of fuel:	300 K
temperature of air:	750 K
combustor pressure:	3.8 atm

The fuel used in the experiment was natural gas but for the present investigation was assumed to be pure methane. Also, dry air was assumed. The experimental data include radial profiles taken at usually four axial stations, of selected species concentrations (measured using a traversing gas sampling probe), temperature (measured by a traversing thermocouple), and axial velocity (measured by laser Doppler velocimetry).

Figure 4 also shows a schematic of the flame configuration observed in the experiment. Because of the high air/fuel velocity ratio, a strong central recirculation zone is formed directly in front of the fuel port, which appears to the surrounding air stream almost as a bluff body. The recirculating combustion products provide a continuous ignition source for the relatively cold incoming reactants, thereby stabilizing the flame. This is different from an unconfined lifted jet flame in which there is no such recirculation zone, and flame stabilization is based on the propagation of triple flames into the unburned mixture; therefore, the performance of the flamelet/progress-variable approach in the current test case should not be generalized to the case of unconfined lifted jet flames. The flame location, shown as a thick convoluted line in figure 4, was observed in the experiment to lift off from the burner and reattach intermittently, in a highly unsteady manner. The length of the flame extended beyond the experimental test section, as well as the computational domain used for the simulations.

The experimentally reported species concentrations were post-processed in order to facilitate comparison with the simulation results. The mole fractions reported in the laboratory report were converted to mass fractions, and mixture fraction and product mass fraction were computed. The following procedure was used. Data were reported for the mole fractions of O_2, CH_4, CO_2, CO, and NO. Mole fractions for the species H_2O and H_2 were assumed to follow stoichiometric relationships: $x_{H_2O} = 2x_{CO_2}$ and $x_{H_2} = 2x_{CO}$. An estimate of the nitrogen mole fraction was obtained from the total oxygen atom mole fraction: $x_{N_2} = 1.88(2x_{O_2} + 2x_{CO_2} + x_{H_2O} + x_{CO})$. Then, mass fractions were computed by neglecting NO and all other species. Mixture fraction was computed based on the total carbon and hydrogen atom mass fractions, and product mass fraction was computed from $y_P = y_{CO_2} + y_{H_2O}$. The validity of these assumptions was tested by performing the same operations on data in the flamelet library and comparing the resulting estimates with the true values. For the ranges of interest, the most unfavourable deviations were approximately $+0.02$ and -0.01 for mixture fraction and $+0.01$ and -0.03 for the progress variable, y_P. The six data points for the CH_4 mole fraction in the fuel-rich region at the first measurement station were not provided because the concentrations were higher than the maximum calibration range of the gas analyser. These missing data were filled in using the above assumptions and the requirement that mole fractions should sum to unity.

6. Computational setup

A picture of the grid used for all of the simulations is shown in figure 5. The distribution of the grid satisfies the general requirements that the grid be smooth and be refined near solid boundaries and in particular in the axial direction at the jet orifice. The thinness of the annular wall separating fuel and air required that especially fine radial resolution be used there. The size of the grid was $256 \times 150 \times 64$ points in the axial, radial, and azimuthal directions, respectively, and was determined by cost considerations as the largest grid on which the simulations could be completed in a reasonable amount of time.

The simulations were computed using length (R), velocity (U), and time (R/U) scales normalized by the injector radius ($R \equiv R_3$) and the inlet bulk velocity of the air

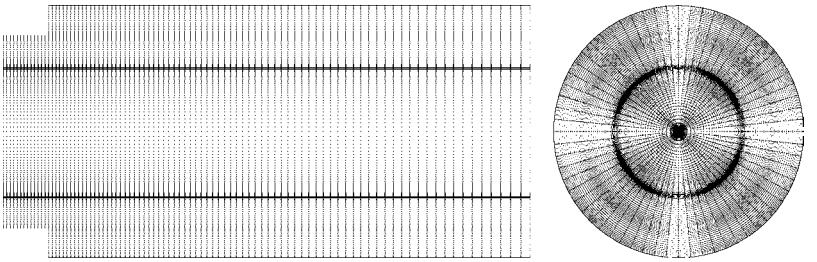

FIGURE 5. Schematic of the grid used for the simulations. Only half of the points in the axial and radial directions are shown for clarity.

($U \equiv V_2$). All simulation results are presented and compared with the experimental data using these units. The computational domain started at a distance of $1R$ upstream of the combustor, where fully developed turbulent inflow conditions were specified using the method described above, even though the experimental inflow conditions were probably not fully developed. The computational domain continued until a combustor length of $8R$ was reached, at which point convective outflow boundary conditions were specified. All of the solid boundaries were assumed to be adiabatic and impermeable, including the annular splitter plate, even though the combustor walls in the experiment were isothermal.

Solutions to the one-dimensional reaction-diffusion equations were computed using GRI-MECH 3.0 and multicomponent mass diffusion, including Soret and Dufour effects for completeness. For the progress-variable approach, product mass fraction ($y_P = y_{CO_2} + y_{H_2O}$) was chosen to serve as the progress variable. The log-normal distribution for dissipation rate was used with the steady-flamelet model.

A time step of 0.005 R/U was used for all of the simulations.

All of the statistical results obtained from the simulations are based on simple averages of the resolved fields in time and in the azimuthal direction. No attempt was made to account for subgrid contributions to the statistics or to account for any effects due to the implicit Favre filtering. Because of the long time scales present in the combustor, a large number of time steps was required to integrate the flow long enough to obtain reasonably converged statistics. The total time needed for initial flow development as well as statistical sampling was about 500 R/U time units or 100 000 time steps for each simulation. The simulations were run on the ASCI Red platform (Sandia National Laboratory, Albuquerque, New Mexico) using 512 processors, yielding a sustained aggregate performance of 10 Gflops, or about 3.7 seconds per time step. Thus, about 50 000 processor-hours were used per simulation.

The flamelet/progress-variable approach has also been used to perform simulations of this same experiment using the unstructured LES code of Mahesh *et al.* (2002) with a grid of approximately 1.3 million cells. These simulations were found to give similar results for the distribution of mixture fraction and progress variable to the structured simulation, indicating that the performance of the model is not sensitive to specific details of the numerical algorithm or the grid.

7. Results

A total of three large eddy simulations of the coaxial jet combustor described in § 5 were performed, each configured with exactly the same computational parameters, but using a different chemistry model: (*a*) fast-chemistry, (*b*) steady-flamelets, and (*c*) progress-variable approach. These simulations are compared with experimental

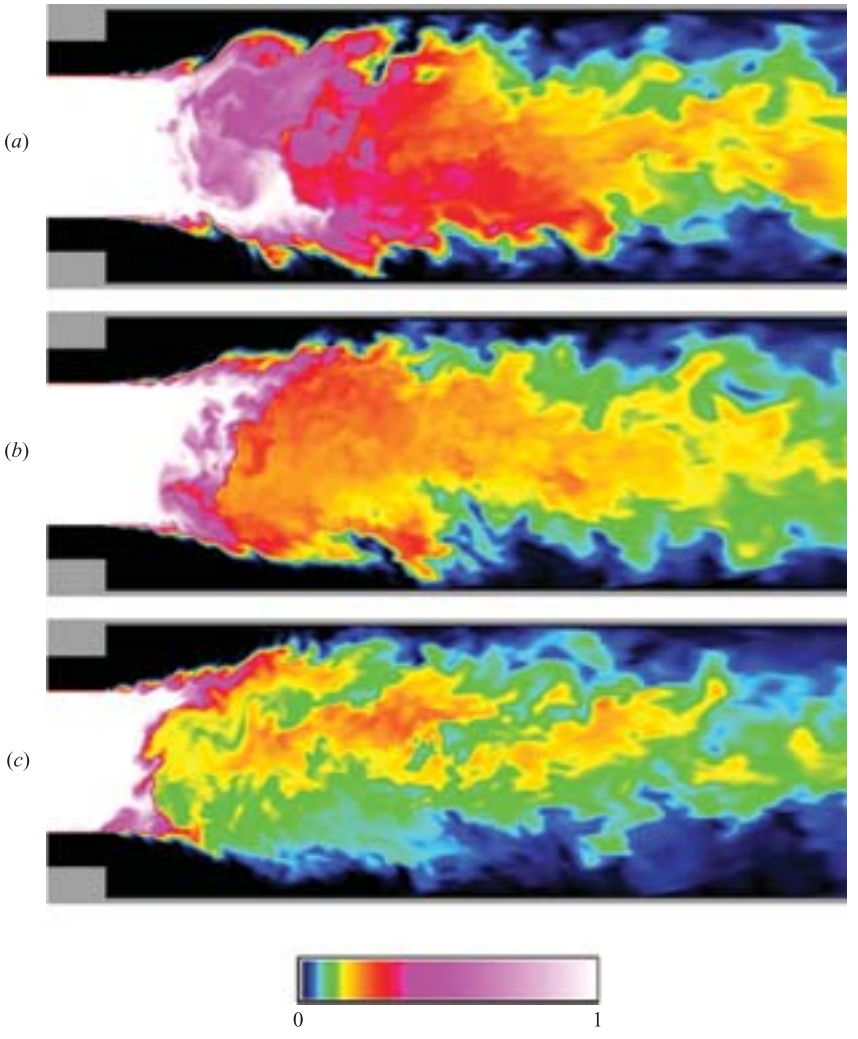

FIGURE 6. Snapshot of mixture fraction in a meridional plane: (*a*) fast-chemistry; (*b*) steady-flamelets; (*c*) progress-variable approach.

data. It is found that both the fast-chemistry and steady-flamelet models fail to account for extinction and flame lift-off close to the burner, while the progress-variable approach predicts a lifted flame and obtains good agreement with the experimental data.

The most important question to be answered is whether the simulation methodology is capable of accurately capturing the gross characteristics and behaviour of the flame, such as the rate of product formation and heat release, flame lift-off, ignition, and extinction. Characteristics that depend on the details of the combustion process, such as pollutant formation, are not a target of the present effort. The primary quantities that are used to examine the characteristics of each simulation are the mixture fraction (Z) and product mass fraction ($y_P = y_{CO_2} + y_{H_2O}$).

7.1. *Instantaneous fields*

Figure 6 compares instantaneous, planar snapshots of mixture fraction for each of the chemistry models: (*a*) fast-chemistry, (*b*) steady-flamelet, and (*c*) progress-variable

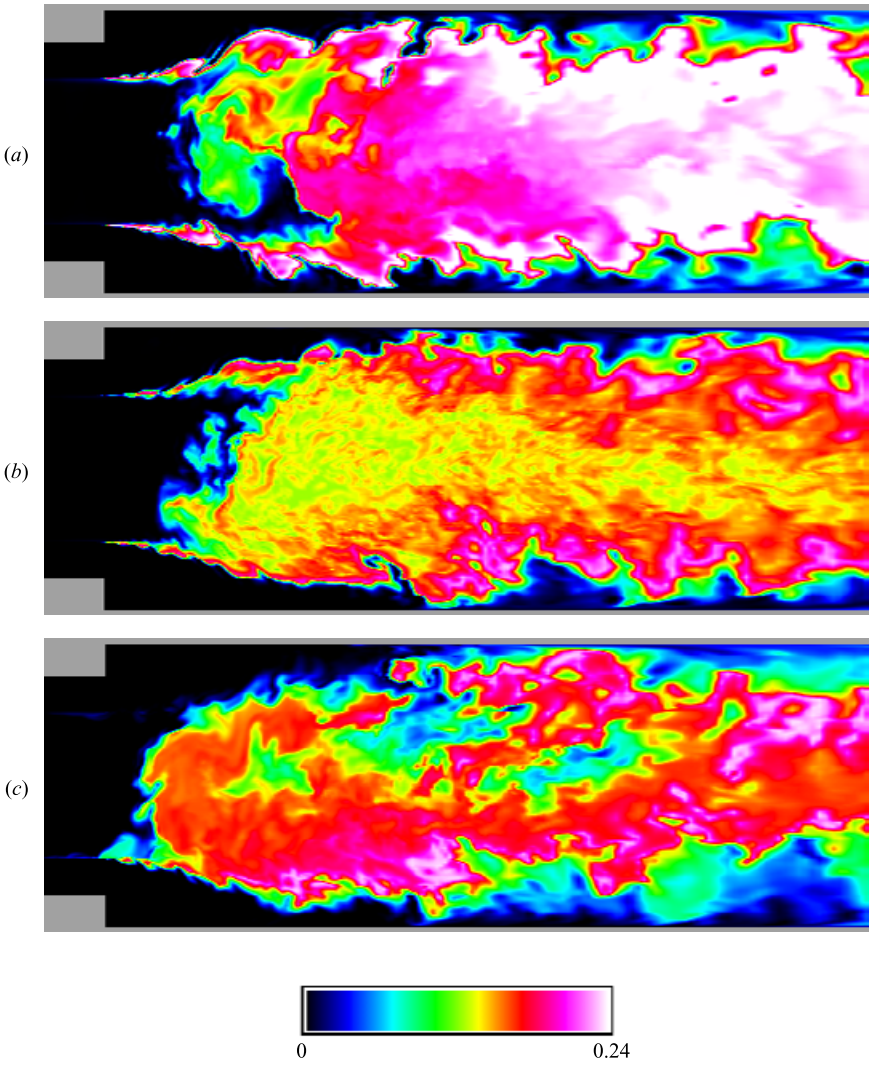

FIGURE 7. Snapshot of product mass fraction in a meridional plane: (*a*) fast-chemistry; (*b*) steady-flamelets; (*c*) progress-variable approach.

approach. Since the three simulations are configured identically except for the chemistry model, and since mixture fraction is a conserved scalar, which does not participate in chemical reactions, one might expect the mixture fraction results for the three cases to be very similar. But scalar mixing can be strongly influenced by heat release, which depends directly on the chemistry model. This is because heat release causes flow dilatation to occur within the thin mixing layers between fuel and oxidizer, thereby pushing apart fuel and oxidizer when they try to mix. In general, the rate of mixing is found to decrease with higher rates of chemical heat release, so that mixture fraction can be used as an indicator of whether the location and rate of chemical reactions are accurately predicted by the chemistry model. The effect of heat release on mixing is clearly visible when comparing the mixing characteristics in the initial thin mixing layers just after the annular splitter plate in figure 6(*a*, *b*), where mixing appears weak, and in figure 6(*c*), where small rollers are visible.

The general conclusion to be drawn from figure 6 is that, of the three chemistry models tested, the fast-chemistry model has the lowest rate of mixing, the progress-variable approach has the highest, and the rate of mixing with the steady-flamelet model lies somewhere between the other two, all due to the resulting heat release rate.

Corresponding pictures of product mass fraction are shown in figure 7. Flame location is identified by the regions of highest product concentration, typically appearing as thin corrugated white lines. Both the fast-chemistry and steady-flamelet models clearly have attached flames, while the progress-variable approach shows a much more complicated and asymmetric pattern: at the particular instant shown, the flame is lifted on the upper side of the injector and is intermittently attached on the lower side. This behaviour is highly unsteady and must be viewed as an animation to be fully appreciated. Because of the extinction occurring on the upper side, unburned reactants are able to penetrate into the interior of the flame as indicated by the darker areas in the centre of figure 7(*c*). The small amounts of product visible in the inlet region of the fuel port are due to occasional recirculation of hot products inside the inlet. In figure 7(*a*), the fast-chemistry model always predicts the theoretical maximum product mass fraction for the given mixture fraction. The highest product mass fraction possible is approximately $y_P = 0.275$ and occurs at the stoichiometric mixture fraction, $Z_{st} = 0.0552$, when all fuel and oxidizer have been converted into product. In figure 7(*b*), the steady-flamelet model predicts significantly lower product mass fractions than the theoretical maximum. This is due to the 'quenching' effect that scalar dissipation rate has on diffusion flame structure. The steady-flamelet model also shows numerous small-scale, wavy structures throughout the central region. These variations should be considered unphysical and a defect of the steady-flamelet model, because they are due solely to local fluctuations in dissipation rate in a region where there is mixing between product and fuel but little or no reaction. In flamelet theory, it is the dissipation rate occurring at the flame surface (the 'stoichiometric' dissipation rate) that controls the flame structure. Accordingly, the description of chemical states in regions away from the flame is not well defined because the steady-flamelet model has no way of creating a non-local connection between a given physical location of arbitrary mixture fraction and a particular physical location of stiochiometric mixture fraction. In the progress-variable approach, this type of non-local interaction is mediated by the progress-variable transport equation.

7.2. *Mixture fraction*

Figure 8 shows quantitatively what is observed qualitatively in figure 6: that the fast-chemistry and steady-flamelet models lead to lower mixing rates because of faster heat release, especially in the thin mixing layers close to the annular splitter plate. The steady-flamelet model clearly offers substantial improvement over the fast-chemistry model, but because it is also incapable of properly accounting for flame lift-off, the mixing profiles remain far above the experimental data. Note that all the profiles tend toward agreement as the profile station is moved farther downstream, due to the fact that they all must reach the same uniform profile once mixing is complete. Since most chemical quantities are correlated with mixture fraction, it is usually important to accurately predict mixture fraction profiles in order to accurately predict other chemical quantities. The scatter of the experimental data points in this and the following figures is due to the reflection about the centreline of data points taken on the opposite side of the combustor.

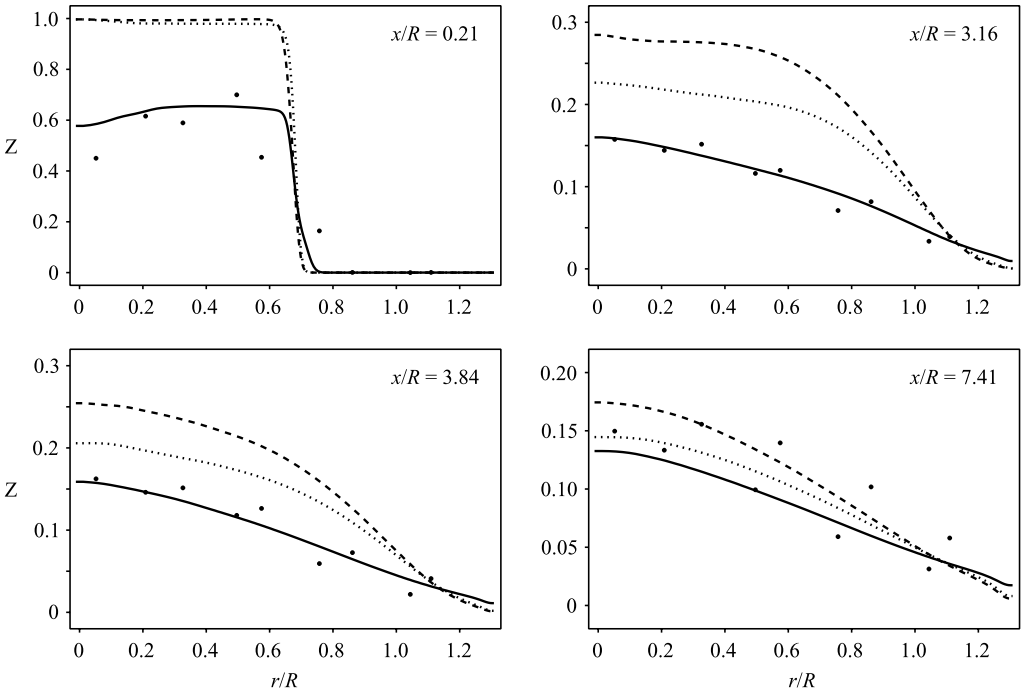

FIGURE 8. Radial profiles of time-averaged mixture fraction: – – – –, fast-chemistry; ·····, steady-flamelets; ——, progress-variable approach; •, experiment.

7.3. *Product mass fraction*

The quantitative picture corresponding to figure 7 is shown in figure 9. The first station clearly shows the similarity between the fast-chemistry and steady-flamelet models and their essential difference with the progress-variable approach. Both the fast-chemistry and steady-flamelet models predict large product formation in the thin mixing layers near the annular splitter plate, as would be expected from an attached flame, while the progress-variable approach has no such spike: the product concentration found at this station is due mainly to recirculation of products from reactions occurring farther downstream. At the remaining stations, the fast-chemistry model consistently overpredicts the levels of product concentration, while the steady-flamelet model and progress-variable approach both achieve good agreement with the experimental data, though it is difficult to say whether one is more accurate than the other because of the scatter in the experimental data.

7.4. *Temperature*

Comparison of predicted temperature profiles with experimental data is shown in figure 10. Temperature is a quantity that is derived from the mixture fraction and progress variable (mixture fraction alone in the fast-chemistry and steady-flamelet models) by assuming adiabatic walls and neglecting thermal radiation. Where these assumptions are valid, the temperature can be expected to behave very similarly to product mass fraction, but where the assumptions break down, an overprediction of temperature is expected. Therefore, if product mass fraction predictions are in good agreement with experimental data, discrepancies between predicted and measured temperature profiles must be due to the breakdown of these assumptions or to experimental error, which owing to differences in measurement technique between

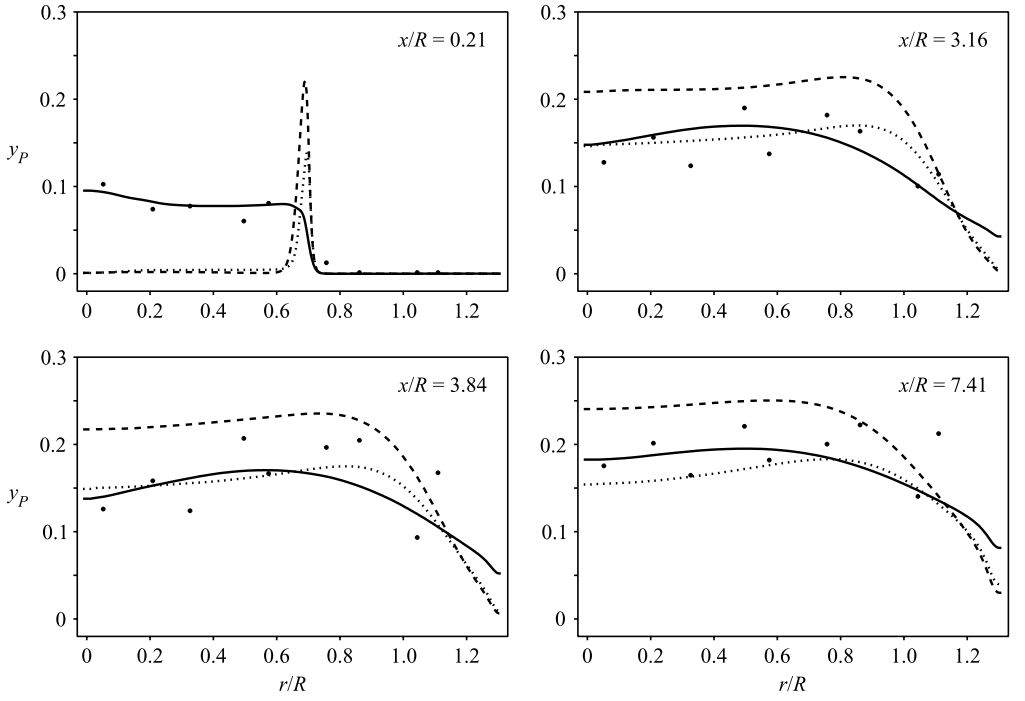

FIGURE 9. Radial profiles of time-averaged product mass fraction: – – –, fast-chemistry; ·····, steady-flamelets; ———, progress-variable approach; •, experiment.

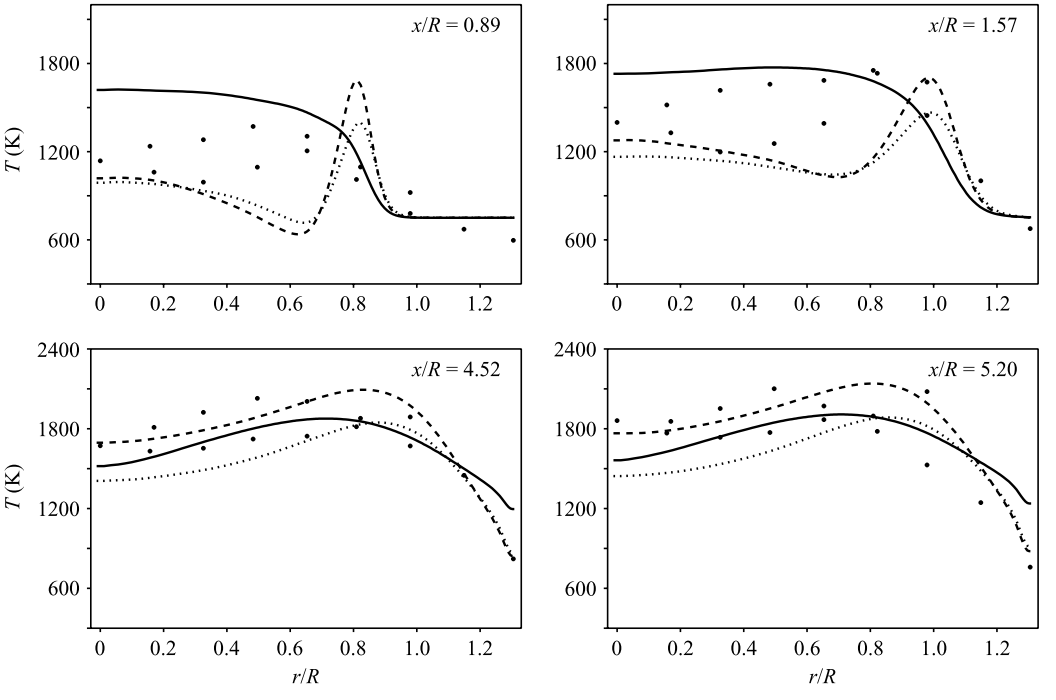

FIGURE 10. Radial profiles of time-averaged temperature: – – –, fast-chemistry; ·····, steady-flamelets; ———, progress-variable approach; •, experiment.

species concentrations and temperature can be significant. One of the investigators involved with the experiment has stated that the temperature data, having been measured using a rather large, invasive, and dynamically unresponsive thermocouple probe, are in fact subject to considerable experimental uncertainty, especially in regions with large temperature fluctuations (C. T. Bowman, private communication, 2001). It could also be the case that thermal radiation is non-negligible in some regions of the flow, particularly in fuel-rich, slow-moving regions where soot formation is likely and residence times are long enough for radiative effects to accumulate. It is also important to note that the axial measurement stations used for temperature are different from those used for species concentrations. In particular, the first two temperature stations are located between the first and second species measurement stations. Thus, the discrepancy between the progress-variable approach and experimental data at the first two temperature stations may in fact reflect an underlying overprediction of product concentration as well, but since species data are not available in this region, it is difficult to draw any definitive conclusions.

Another source of uncertainty is the effect of the assumption of adiabatic walls in the simulations. Since the experiment had isothermal, water-cooled walls at roughly 500 K, thermal boundary layers would be expected to develop, affecting the temperature close to the wall. However, note that in figure 7, the annular air stream (at 750 K) tends to create an insulating sheath between the hot combustion products and the wall, although it appears that the flame in figure 7(*c*) does occasionally brush against the wall. These factors should account for the good agreement of the fast-chemistry and steady-flamelet models, and the overprediction of the progress-variable approach near the wall at the last two stations in figure 10.

7.5. *Velocity*

Time-averaged axial velocity and axial fluctuation intensity results are shown in figure 11. While scalar mixing was found to be sensitive to the heat release characteristics of the chemistry model, surprisingly the time-averaged velocity field data are rather insensitive. In fact, the velocity data for the fast-chemistry and steady-flamelet models were found to be nearly indistinguishable. As the effects of heat release on the velocity field tend to be cumulative, velocity field differences between the three models can be expected to increase with axial distance. Indeed, the only significant difference between the fast-chemistry, steady-flamelet, and progress-variable velocity fields appears at the final measurement station, where the progress-variable approach achieves significantly better agreement with the experiment.

The general level of agreement between simulation and experiment is satisfactory but not quite as good as has been achieved with LES of incompressible turbulent flows. A significant part of the disagreement may be due to the fact that fully developed pipe and annular inflow conditions were assumed in the simulations, whereas in the experiment, flow conditioning devices were located only a short distance upstream of the jet orifice.

Finally, it should be noted that the axial location of the third measurement station was reported to be '0.187 X/D' (0.49 x/R), where 'D' is the diameter of the combustor. But based on the plausible rate of change of the flow patterns in the axial direction and other information contained in the report, this value was suspected of being a typographical error and was corrected to its most probable value of '0.487 X/D' (1.27 x/R).

7.6. *Carbon monoxide*

Figure 12 presents the CO results for the steady-flamelet model and progress-variable approach. Note that the fast-chemistry model with the major products assumption

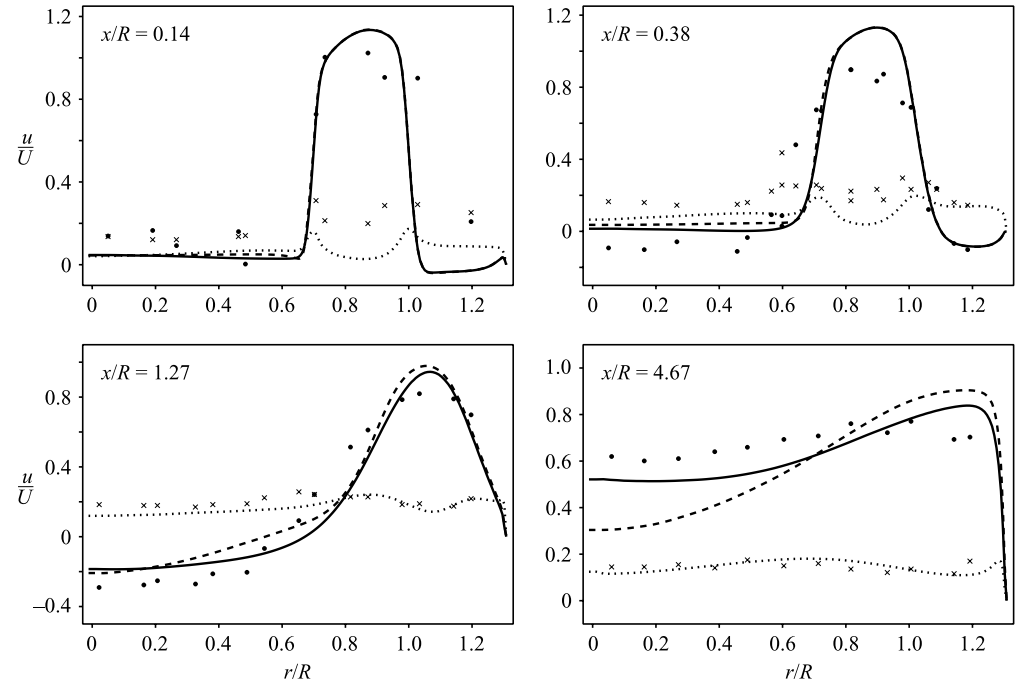

FIGURE 11. Radial profiles of time-averaged axial velocity and axial fluctuation intensity: – – – –, $\bar{u}$, both fast-chemistry and steady-flamelet models; ———, $\bar{u}$, progress-variable approach; ·····, $\sqrt{\overline{u'^2}}$, progress-variable approach; •, $\bar{u}$, experiment; ×, $\sqrt{\overline{u'^2}}$, experiment.

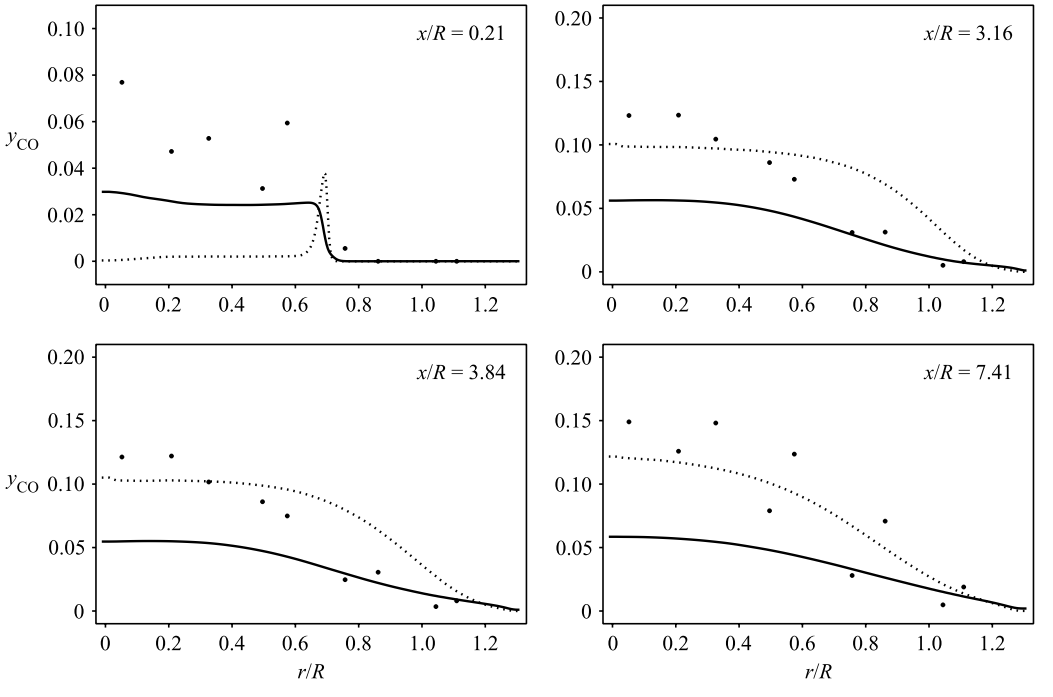

FIGURE 12. Radial profiles of time-averaged CO mass fraction. ·····, steady-flamelets; ———, progress-variable approach; •, experiment.

predicts zero carbon monoxide concentrations. The results clearly show that the progress-variable approach has room for improvement, and that in this case, the steady-flamelet model significantly outperforms the progress-variable approach at the last station. Carbon monoxide is a significant species in the fuel-rich interior region of the flame. Because dissipation rates are low in this region, the steady-flamelet model picks out near-equilibrium flamelet solutions, which have low temperatures and high concentrations of CO in fuel-rich mixtures. But this part of the flamelet library is not uniquely mapped by the progress variable, so that such high-CO chemical states cannot be accessed. One possible improvement is to consider using entropy as the progress variable, as entropy always increases monotonically as reactions progress towards equilibrium.

8. Conclusions

Large-eddy simulation was shown to be a promising technique for prediction of complex turbulent reacting flows. Motivated by the inability of existing chemistry models to predict lifted diffusion flames, such as those occurring in gas turbine combustors, a new two-scalar approach involving mixture fraction and a reaction progress variable was developed. This is combined with a steady-flamelet model that incorporates detailed chemical kinetics and multicomponent mass diffusion.

The calculations were compared with detailed experimental data from the United Technologies Research Center. Excellent agreement was obtained between computations and the experiment in the mean and fluctuating velocity profiles, mean mixture fraction profiles, and mean product concentration. This agreement is particularly significant because no adjustable parameters were available for tuning, owing to the use of the dynamic procedure in the parameterization of turbulence.

Three chemistry models were tested in the present study: fast-chemistry, steady-flamelet, and the progress-variable approach. The progress-variable approach appears to be an effective method for capturing basic realistic flame behaviour such as flame lift-off while requiring only a marginal increase in computational cost compared to the other two models. However, the present formulation cannot accurately predict details of the combustion process such as pollutant formation and thermal radiation, and thus, future improvements will be necessary.

This paper is based on the doctoral dissertation of Charles David Pierce at Stanford. Charles passed away on March 25, 2002. I am grateful to Professor Heinz Pitsch, Cliff Wall, and Lee Shunn for their help in the preparation of this manuscript for publication. We felt the legacy of Charles' enormous creativity and pioneering contribution to turbulent combustion will be preserved by this publication in the archival literature.

This project was supported by the AFOSR Turbulence Program, the Franklin and Caroline Johnson Graduate Fellowship at Stanford and NASA.

REFERENCES

Akselvoll, K. & Moin, P. 1996 Large-eddy simulation of turbulent confined coannular jets. *J. Fluid Mech.* **315**, 387–411.

Bushe, W. K. & Steiner, H. 1999 Conditional moment closure for large eddy simulation of nonpremixed turbulent reacting flows. *Phys. Fluids* **11**, 1896–1906.

Chen, M., Herrmann, M. & Peters, N. 2000 Flamelet modeling of lifted turbulent methane/air and propane/air jet diffusion flames. *Proc. Combust. Inst.* **28**, 167–174.

Colucci, P. J., Jaberi, F. A., Givi, P. & Pope, S. B. 1998 Filtered density function for large eddy simulation of turbulent reacting flows. *Phys. Fluids.* **10**, 499–515.

Cook, A. W. 1997 Determination of the constant coefficient in scale similarity models of turbulence. *Phys. Fluids* **9**, 1485–1487.

Cook, A. W. & Riley, J. J. 1994 A subgrid model for equilibrium chemistry in turbulent flows. *Phys. Fluids* **6**, 2868–2870.

Cook, A. W., Riley, J. J. & Kosály, G. 1997 A laminar flamelet approach to subgrid-scale chemistry in turbulent flows. *Combust. Flame* **109**, 332–341.

DesJardin, P. E. & Frankel, S. H. 1998 Large eddy simulation of a turbulent nonpremixed reacting jet: Application and assessment of subgrid-scale combustion models. *Phys. Fluids* **10**, 2298–2314.

Domingo, P., Vervisch, L. & Bray, K. 2002 Partially premixed flamelets in LES of nonpremixed turbulent combustion. *Combust. Theory Modelling* **6**, 529–551.

Frankel, S. H., Adumitroaie, V., Madnia, C. K. & Givi, P. 1993 Large eddy simulation of turbulent reacting flows by assumed PDF methods. In *Engineering Applications of Large Eddy Simulations* (ed. S. A. Ragab & U. Piomelli), pp. 81–101. ASME.

Gao, F. & O'Brien, E. E. 1993 A large-eddy simulation scheme for turbulent reacting flows. *Phys. Fluids* A **5**, 1282–1284.

Germano, M., Piomelli, U., Moin, P. & Cabot, W. H. 1991 A dynamic subgrid-scale eddy viscosity model. *Phys. Fluids* A **3**, 1760–1765.

Jaberi, F. A., Colucci, P. J., James, S., Givi, P. & Pope, S. B. 1999 Filtered mass density function for large-eddy simulation of turbulent reacting flows. *J. Fluid Mech.* **401**, 85–121.

Jaberi, F. A. & James, S. 1998 A dynamic similarity model for large eddy simulation of turbulent combustion. *Phys. Fluids* **10**, 1775–1777.

Jiménez, J., Liñán, A., Rogers, M. M. & Higuera, F. J. 1997 *A priori* testing of subgrid models for chemically reacting non-premixed turbulent shear flows. *J. Fluid Mech.* **349**, 149–171.

Johnson, B. V. & Bennett J. C. 1984 Statistical characteristics of velocity, concentration, mass transport, and momentum transport for coaxial jet mixing in a confined duct. *J. Engng Gas Turbines and Power* **106**, 121–127.

Klimenko, A. Y. & Bilger, R. W. 1999 Conditional moment closure for turbulent combustion. *Prog. Energy Combust. Sci.* **25**, 595.

Legier, J. P., Poinsot, T. & Veynante, D. 2000 Dynamically thickened flame LES model for premixed and non-premixed turbulent combustion. *Proc. 2000 CTR Summer Program*, pp. 157–168. Center for Turbulence Research, NASA-Ames/Stanford University.

Lesieur, M. & Métais, O. 1996 New trends in large-eddy simulations of turbulence. *Annu. Rev. Fluid Mech.* **28**, 45–82.

Mahesh, K., Constantinescu, G., Apte, S., Iaccarino, G., Ham, F. & Moin, P. 2002 Progress toward large-eddy simulation of turbulent reacting and non-reacting flows in complex geometries. *CTR Annual Research Briefs*, Center for Turbulence Research, NASA Ames/Stanford University.

Moin, P. 2002 Advances in large eddy simulation methodology for complex flows. *Intl J. Heat Fluid Flow* **23**, 710–720.

Moin, P., Squires, K., Cabot, W. & Lee, S. 1991 A dynamic subgrid-scale model for compressible turbulence and scalar transport. *Phys. Fluids* A **3**, 2746–2757.

Müller, C. M., Breitbach, H. & Peters, N. 1994 Partially premixed turbulent flame propagation in jet flames. *Proc. Combust. Inst.* **25**, 1099–1106.

van Oijen, J. A. & de Goey, L. P. H. 2002 Modelling of premixed counterflow flames using the flamelet-generated manifold method. *Combust. Theory Modelling* **6**, 463–478.

Owen, F. K., Spadaccini, L. J. & Bowman, C. T. 1976 Pollutant formation and energy release in confined turbulent diffusion flames. *Proc. Combust. Inst.* **16**, 105–117.

Peters, N. 1984 Laminar diffusion flamelet models in non-premixed turbulent combustion. *Prog. Energy Combust. Sci.* **10**, 319–339.

Peters, N. 2000 *Turbulent Combustion.* Cambridge University Press.

Pierce, C. D. & Moin, P. 1998*a* Large eddy simulation of a confined coaxial jet with swirl and heat release. *AIAA Paper* 98-2892.

Pierce, C. D. & Moin, P. 1998*b* Method for generating equilibrium swirling inflow conditions. *AIAA J.* **36**, 1325–1327.

Pierce, C. D. & Moin, P. 1998*c* A dynamic model for subgrid-scale variance and dissipation rate of a conserved scalar. *Phys. Fluids* **10**, 3041–3044.

Pierce, C. D. & Moin, P. 2001 Progress-variable approach for large-eddy simulation of turbulent combustion. *Mech. Eng. Dept. Rep.* TF-80. Stanford University.

Pitsch, H. & Steiner, H. 2000 Large-eddy simulation of a turbulent piloted methane/air diffusion flame (Sandia flame D). *Phys. Fluids* **12**, 2541–2554.

Réveillon, J. & Vervisch, L. 1996 Subgrid-scale turbulent micromixing: dynamic approach. *AIAA J.* **36**, 336–341.

Spadaccini, L. J., Owen, F. K. & Bowman, C. T. 1976 Influence of aerodynamic phenomena on pollutant formation in combustion (Phase I. Gaseous fuels). *U.S. Environmental Protection Agency Rep.* EPA-600/2-76-247a.

Steiner, H. & Bushe, W. K. 2001 Large eddy simulation of a turbulent reacting jet with conditional source-term estimation. *Phys. Fluids* **13**, 754–769.

Vervisch, L. & Trouvé, A. 1998 LES modeling for lifted turbulent jet flames. *Proc. 1998 CTR Summer Program*, pp. 83–100. Center for Turbulence Research, NASA-Ames/Stanford University.

Wall, C., Boersma, B. J. & Moin, P. 2000 An evaluation of the assumed beta probability density function subgrid-scale model for large eddy simulation of nonpremixed, turbulent combustion with heat release. *Phys. Fluids* **12**, 2522–2529.

Wall, C., Pierce, C. D. & Moin, P. 2002 A semi-implicit method for resolution of acoustic waves in low Mach number flows. *J. Comput. Phys.* **181**, 545–563.